Preparation and In Vitro Analysis of Dendrimer-encapsulated Liposomes

BY

ERI IWASAKI
B.S. in Applied Chemistry, Ehime University 2009

THESIS

Submitted as partial fulfillment of the requirements
for the degree of Master of Science in Bioengineering
in the Graduate College of the
University of Illinois at Chicago, 2013

Chicago, Illinois

Defense committee:

Seungpyo Hong, Chair and Adviser
David Eddington
Richard Gemeinhart, Biopharmaceutical Sciences

Table of contents

List of tables iv
List of figures v
List of abbreviations vi
Summary viii
1. Introduction 1
1.1 Drug delivery 1
1.2 Cancer physiology and two targeting strategies 2
1.3 Dendrimer-membrane interactions 3
1.4 PEGylated liposomes and their applications in nanomedicine 3
1.5 Roles of cholesterol on liposomes and plasma membranes 4
1.6 Dendrimer-liposome interactions 6
2. Materials and methods 7
2.1 Preparation and characterization of G2-RITC 7
2.2 Encapsulation of G2 conjugates into liposomes 8
2.3 Characterization of dendrimer-encapsulated liposomes 9
2.4 Morphology of the liposomes: TEM observation 10
2.5 Release kinetics of G2-RITC-NH_2 from liposomes 10
2.6 Cell Culture 10
2.7 Optimization of G2 concentration for cellular uptake experiments 11
2.8 Cellular uptake of G2-RITC-NH_2: Fluorescence microscopy observations 11
2.9 Effect of low-temperature on G2-RITC-NH_2 internalizations 11
2.10 Cellular uptake of G2-RITC-NH_2: Flow cytometry measurements 12
2.11 Cellular interactions of liposomes following MβCD treatment 12
2.12 Cytotoxicity of dendrimer-encapsulated liposomes 13
3. Results and discussion 14
3.1 Characterization of dendrimer-encapsulated liposomes 14
3.2 Release kinetics of dendrimer-encapsulated liposomes 16
3.3 Cellular uptake of dendrimer-encapsulated liposomes 18

3.4 Cytotoxicity of dendrimers and dendrimer-encapsulated liposomes.....25
4. Conclusion 28
References.....30
Vita.....32

List of tables

Table 1. Characterization of G2-RITC-NH_2-encapsulated liposomes.....23

List of figures

Figure 1. Conjugation of Rhodamine B Isothiocyanate 15

Figure 2. Encapsulation of G2-RITC-NH_2 into liposomes consisting of DMPC, DSPE-PEG2000, and cholesterol 17

Figure 3. Standard curve generated from dendrimer fluorescence versus concentration in 0.1% Triton X-100. The standard yielded $R^2 = 0.9974$ and an equation $y=138.79x + 37.416$ 22

Figure 4. Transmission electron microscopy (TEM) images of dendrimer-encapsulated liposomes (Contributed by Ryan M. Pearson) 23

Figure 5. Standard curve generated from dendrimer fluorescence versus concentration in PBS. The standard yielded $R^2 = 0.9994$ and an equation $y=122.81x + 32.4$ 24

Figure 6. Release kinetics in PBS of a) G2-RITC-NH_2-encapsulated liposomes consisting of DMPC and cholesterol, and b) PEI-RITC- and G2-RITC-NH_2-encapsulated liposomes consisting of DSPC, DOPG, and cholesterol 26

Figure 7. Cellular uptake images of different concentrations (100-100 nM) of G2-RITC-NH_2 after 3 and 6 h (BF: bright field images, FL: fluorescent images) 27

Figure 8. Cellular uptake images of MCF-7 cells following treatment with G2-RITC-NH_2 and the three liposomal formulations (liposomes with 25% cholesterol, liposomes with 50% cholesterol, and liposomes with 75% cholesterol) at a concentration of 500 nM based on G2-RITC-NH_2 for 4 and 24 h (BF: bright field images, FL: fluorescent images). 28

Figure 9. Cellular uptake images of G2-RITC-NH_2 and the three liposomal formulations after 4 h incubation at 4℃ (BF: bright field images, FL: fluorescent images) 30

Figure 10. Cellular uptake of G2-RITC-NH_2 and the three liposomal formulations after 4 h incubation at a) 37℃ and b) 4℃. 31

Figure 11. Kinetics of cellular uptake of G2-RITC-NH_2 and three liposomes in the a) absence and b) presence of MβCD. 32

Figure 12. Cytotoxicity of G2-RITC-NH_2 and G2-RITC-NH_2-encapsulated liposomes after incubation with MCF-7 cells for a) 1 h, b) 4 h, c) 24 h, and d) 48 h at a concentration equivalent to 0.1, 0.5, 1, and 10 μM G2-RITC-NH_2. 34

Figure 13. Cytotoxicity of G2-RITC-NH_2 after incubation with MCF-7 cells at concentrations of 10, 100, and 500 μM up to 48 h. 35

List of abbreviations

CLSM	Confocal laser scanning microscope
DCM	Dichloromethane
DMPC	1,2-dimyristoyl-*sn*-glycero-3-phosphocholine
DMSO	Dimethyl sulfoxide
DOPG	1,2-dioleoyl-*sn*-glycero-3-phospho-(1'-rac-glycerol)
DSPC	1,2-distearoyl-*sn*-glycero-3-phosphocholine
DSPE-PEG-2000	1,2-Distearoyl-sn-glycero-3-phosphoethanolamine-N-mPEG-2000
ECM	Extracellular matrix
EPR	Enhanced permeability and retention
FA	Folic acid
FACS	Fluorescence activated cell sorting
FR	Folic acid receptor
G2	Generation 2 Poly(amidoamine) (PAMAM) dendrimers
HSPC	Hydrogenated soy phosphatidylcholine
KB FR^+	FR-overexpressing KB cells
MβCD	methyl-beta-cyclodextrin
MWCO	Molecular weight cut off
NPs	Nanoparticles
PBS	Phosphate buffered saline
PC	L-α-phosphatidylcholine
PEG	Poly(ethylene glycol)
PEI	Polyethylenimine

PPE	Palmar Plantar Erythrodysesthesia
PTA	Phosphotungstic acid
RES	Reticuloendothelial system
RITC	Rhodamine B isothiocyanate
TEM	Transmission electron microscopy
T_m	Phase transition temperature

Summary

Rhodamine B isothiocyanate (RITC) labeled generation 2 Poly(amidoamine) (PAMAM) dendrimers (G2-RITC-NH_2) were encapsulated into liposomes consisting of 1,2-dimyristoyl-*sn*-glycero-3-phosphocholine (DMPC), 1,2-Distearoyl-sn-glycero-3-phosphoethanolamine-N-mPEG-2000 (DSPE-PEG-2000), and cholesterol using a lipid film hydration method. Three different liposomal formulations were prepared by varying the cholesterol content at 25, 50, and 75 mol%. The prepared liposomes showed a size range of 160-180 nm. The liposomes were then investigated in terms of (i) release kinetics of G2-RITC-NH_2 from each liposome, (ii) cellular uptake kinetics, (iii) endocytosis mechanisms, and (iv) cytotoxicity. The release profiles of G2-RITC-NH_2 from each liposome revealed that the stability of the liposomes is highly dependent on the cholesterol level in the lipid bilayer. Microscope observations and flow cytometry measurements also showed the different internalization kinetics of the three liposomal formulations from that of unencapsulated G2-RITC-NH_2. In order to further investigate the endocytosis mechanisms of these materials, MCF-7 cells were pre-treated with 5 mM methyl-beta-cyclodextrin (MβCD) before being incubated with unencapsulated G2-RITC-NH_2 and the liposomal formulations up to 24 h. The results obtained from the flow cytometry analysis indicated that G2-RITC-NH_2 internalizes into the cells by a different mechanism compared to the liposomes. Finally, cytotoxicity of G2-RITC-NH_2 and the three liposomal formulations was investigated, which showed no significant inhibition of cell proliferation up to 10 μM normalized based on the G2-RITC-NH_2 concentration, indicating that the materials could be used as a drug delivery platform. In summary, the in vitro characterization experiments conducted in this study serve as a critical starting point to engineer effective drug delivery systems that combine the advantages of dendrimers and liposomes.

1. Introduction

In 2013, about 580,350 Americans are expected to die of cancer, almost 1,600 people per day [1]. Cancer is one of the most common causes of death in the US and characterized by uncontrolled growth and spread of abnormal cells. The 5-year relative survival rate for all cancers diagnosed between 2002 and 2008 is 68%, increased from 49% in 1975-1977 [1]. Most of the currently available chemotherapeutics often come with undesirable side effects due to their toxicity over the normal cells and tissues. In the last few decades, developments in nanotechnology have greatly impacted cancer treatments. By reducing the toxic side effects and altering the biodistribution of drug molecules, polymeric nanoparticles, dendrimers, micelles, and liposomes, have shown great promise as anticancer drug delivery vehicles [2, 3].

1.1 Drug delivery

Since most of currently available cancer chemotherapeutics often come with severe side effects caused by high toxicity to healthy cells and tissues, it is important to design a novel platform to deliver drugs specifically to the target tissue. In order to minimize these side effects, a number of nanoparticle-based therapeutic, including liposomes, polymeric nanoparticles, micelles, dendrimers, and metallic nanoparticles, has been developed in the last few decades [2, 4-6]. Consequently, application of these nanotechnology in the medical field has enhanced the therapeutic activity and reduced the toxic side effects of cancer drugs by improving solubility of hydrophobic drugs, minimizing immunogenicity, and controlling drug circulation time [7]. However, even though an extensive amount of study is ongoing in this field, most research will not achieve clinical use due to various parameters, such as drug loading efficiency, particle size and charge, density of targeting ligands, surface hydrophilicity, and so on [8]. Only a few of

experimental approaches utilizing nanoparticles have met the qualification of clinical use and become commercially available. Engineering a successful delivery platform of therapeutic or diagnostic carriers, therefore, still needs to be developed elaborately.

1.2 Cancer physiology and two targeting strategies

As the rapid development of tumors often causes aberrantly elevated levels of angiogenesis, leaky blood vessels and poor lymphatic drainage are often shown in neovascular networks supplying tumor sites [9, 10]. The leaky blood vessels accelerate the diffusion of drug carriers into the tumor sites and the poor lymphatic drainage in tumors retains those accumulations. Passive targeting approaches rely on this enhanced permeability and retention (EPR) effect. In order to take advantages of passive targeting strategy, carriers are often controlled to be 50-200 nm in size, which have been shown to be effective to extravasate into tumor sites [11-13]. Even though passive targeting strategies meet the basis of clinical use, they still suffer from several limitations. Nanocarriers after extravasation, 50-200 nm in size, do not travel far away from the vessels, and the passive targeting strategies lack cell specific interactions which are necessary to induce internalizations of nanocarriers. Moreover, targeting cancer cells utilizing the EPR effect is not always feasible in all tumors because tumor vascularization and porosity of blood vessels are varying with tumor types [14].

On the other hand, active targeting employs targeting ligands that interact with receptors expressed on the targeted cell surface, which can increase the targeting efficacy of nanocarriers as they actively bind to target cells after extravasation. Active targeting, however, also has the drawback that the surface exposure of targeting ligands can lead to increased unwanted uptake

and rapid clearance [15]. Therefore, in order to achieve a high targeting efficacy, taking advantages of both passive and active targeting is desirable.

1.3 Dendrimer-membrane interactions

Dendrimers are well-defined nanostructured macromolecules that show narrow mass or size polydispersity and possess multifunctionality and high water solubility [16, 17]. Their unique characteristics make dendrimers be a promising candidate for drug, gene, and imaging agent delivery [18-21]. By conjugating target ligands, dendritic nanodevices have been shown to be highly effective in selective tumor targeting via specific interaction between ligands and receptors expressed on the cells. For example, it has been shown by Kukowska-Latallo *et al*. that methotrexate conjugated folic acid (FA)-targeted poly(amidoamine) (PAMAM) dendrimers have significantly lower toxicity and 10-fold higher efficacy compared to free methotrexate at an equal cumulative dose [15].

Hong *et al.* have developed a series of studies on the biological interactions between dendrimers and either lipid bilayers or cell membranes [22-24]. In those studies, it has been found that positively charged PAMAM dendrimers create nano-scale holes in lipid bilayers leading to nonselective internalization into cells, while neutral and negatively charged PAMAM dendrimers do not induce the hole formation. These observations suggested a straightforward explanation for endocytosis mechanisms of PAMAM dendrimers.

1.4 PEGylated liposomes and their applications in nanomedicine

Lipid-based nanoparticles such as liposomes are highly promising drug nanocarriers and widely used for therapeutic drug delivery, including genes, proteins, and imaging agents due to

their superior biocompatibility, encapsulation ability of either hydrophobic or hydrophilic drugs without the conjugation chemistries, and customizable multifunctionality [25-28]. Indeed, the most widely marketed nanomedicines approved by FDA are lipid-based products such as Doxil®, Myocet®, and DaunoXome®. Doxil® consists of a single lipid bilayer membrane composed of hydrogenated soy phosphatidylcholine (HSPC) and cholesterol with doxorubicin encapsulated in the internal compartment [29]. In order to enhance the stability, prevent early leakage of drug from liposomes, and protect from the reticuloendothelial system (RES), poly(ethylene glycol) (PEG) is grafted to the surface of liposomes [29-31]. Consequently, many studies have proven significant therapeutic efficacy of Doxil® in variety tumor animal models and in humans [32-34]. However, side effects that cannot be observed for free doxorubicin are observed for Doxil® such as Palmar Plantar Erythrodysesthesia (PPE) known as "foot and hand syndrome". It is reported that up to 48% of patients prescribed Doxil® suffer from the PPE and the exact mechanism causing PPE is still unknown [35]. Furthermore, there are still debates on the mechanism of doxorubicin release and internalization. Barenholz *et al.* has suggested two different mechanisms: (i) Doxil® itself is internalized into tumor cells, and (ii) free doxorubicin released from liposomes at tumorous extracellular matrix (ECM) is taken up by cells [32]. Although the latter hypothesis is seemingly more predominant due to the liposome destabilization by the ammonium sulfate gradient at the tumor tissues, further investigation of the liposomal formulation, membrane permeability, and cellular interaction is needed for better understanding of liposomal nanocarriers.

1.5 Roles of cholesterol on liposomes and plasma membranes

The fluidity of a lipid bilayer changes with temperature. The lipid bilayer exists in a solid (gel) phase at below the phase transition temperature (T_m) and exists in the liquid phase at the temperature above T_m. In the solid (gel) phase, lipids are packed tightly and the lipid bilayer exhibits a high stability. In the liquid phase, on the other hand, lipids exchange their location with their adjoining lipids millions of times a second and this enhances permeability of bilayers. However, it has been known that the presence of cholesterol induces the stability of liposomes since cholesterol molecules fill in the free space between lipids as a large number of studies have shown [36-40]. Senior *et al.* showed that stability of liposomes containing carboxyfluorescein (CF) in serum was increased by adding cholesterol into liposomal membranes as observed by the reduction of CF leakage from the liposomes. Meanwhile, CF leakage from cholesterol-free liposomes composed of saturated phospholipids was dependent on the T_m of lipid component [40].

Cholesterol in mammalian cell membranes plays a key role in operating normal cellular functions [41]. Cholesterol present in the cell is either transported from low-density lipoproteins, internalized through clathrin-mediated endocytosis, or synthesized in the endoplasmic reticulum [42, 43]. More than 90% of the cellular cholesterol exists in plasma membranes and plays important roles on both the physical properties of membranes such as fluidity, and functional attributes of cells such as the activities of various integral proteins [44]. In addition, it has been known that cholesterol is indispensable for invagination of caveolae and clathrin-coated pits [45-50]. Rothberg *et al*. have reported that folate receptor clustering, guiding the formation of caveolae-coated pits was significantly arrested in the cholesterol-depleted cells by filipin treatment [45]. This observation suggested that cholesterol plays an essential role in retaining a caveolae and inducing a caveolae mediated endocytosis. Furthermore, Rodal *et al.* showed the

importance of cholesterol for endocytosis in HEp-2 cells by extracting cholesterol from the plasma membranes using methyl-β-cyclodextrin (MβCD). Electron microscopy observation revealed that no invaginated caveolaes were present in MβCD-treated HEp-2 cells. More importantly, strong inhibition of invagination of clathrin-coated pits was also observed [46]. These studies clearly indicate that the presence of cholesterol in the plasma membrane is critical for better understanding of endocytosis mechanisms.

1.6 Dendrimer-liposome interactions

Although both dendrimers and liposomes have been used extensively as drug delivery platforms, very little work has been undertaken to investigate interactions between dendrimers and liposomes. The first attempt to incorporate dendrimers into liposomes was done in 2001 [51]. In that study, the interactions between cationic partial dendrimers having three lipidic (C_{14}) chains coupled to dendritic lysine head groups and liposomes with various charges was investigated. Since 2002, the study of dendrimer-encapsulated liposomes has been developed in order to increase the loading efficiency of drugs and control the drug release kinetics. In those studies, it has been found that the loading of drugs increase proportionally to dendrimer generation, while the leakage of the drug from the dendrimer-liposome hybrid system decrease [52, 53]. In our study, in order to investigate the cellular interaction of dendrimer-encapsulated liposomes, we encapsulated G2 PAMAM dendrimers into liposomes with various ratios of DMPC to cholesterol (liposomes with 25%, 50%, and 75% cholesterol). The effects of cholesterol on permeability of liposomes, cellular uptake, internalization mechanisms, and cytotoxicity of both unencapsulated G2-RITC-NH_2 and G2-RITC-NH_2-encapsulated liposomes were investigated.

2. Materials and methods

Generation 2 (G2) PAMAM dendrimer, rhodamine B isothiocyanate (RITC, mixed isomers), cholesterol, dichloromethane (DCM), methanol, and methyl-β-cyclodextrin (MβCD) were all obtained from Sigma-Aldrich (St. Louis, MO). 1,2-Distearoyl-sn-glycero-3-phosphoethanolamine-N-mPEG-2000 (DSPE-PEG-2000), and 1,2-dimyristoyl-*sn*-glycero-3-phosphocholine (DMPC) were all purchased from Avanti Polar Lipids Inc. (Alabaster, AL).

2.1 Preparation and characterization of G2-RITC

G2 PAMAM dendrimer conjugation was performed as previously described [54-56]. Briefly, G2 PAMAM dendrimers (10.0 mg, 3.1 μmol) were dissolved in 1 mL DMSO. RITC (2.5 mg, 4.6 μmol, 50% molar excess to G2) was first dissolved in 200 μL DMSO and then added to the dendrimer solution dropwise under vigorous stirring at RT for 24 h, resulting in G2-RITC-NH_2. Unreacted RITC was removed by membrane dialysis (Spectra/Pro dialysis membrane, MWCO of 500, Spectrum Laboratories Inc., Rancho Dominguez, CA) in 4 L deionized distilled water (ddH_2O) for 3 days. The purified product was lyophilized for 2 days and stored at -20℃.

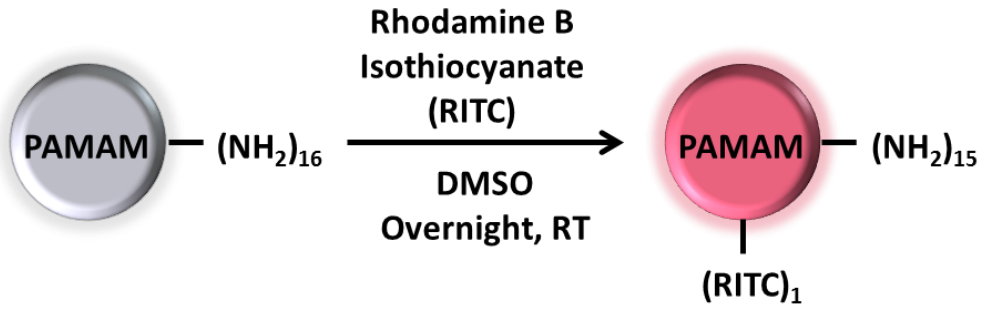

Figure 1. Conjugation of Rhodamine B Isothiocyanate

2.2 Encapsulation of G2 conjugates into liposomes

Unilamellar liposomes consisting of DMPC/cholesterol (75:25, 50:50, and 25:75, mol/mol) were prepared using a film hydration method followed by extrusion as previously described [54]. DSPE-PEG-2000 was added to each liposome at 5 mol% in order to enhance the stearic stability. First, DSPE-PEG-2000, DMPC, and cholesterol were dissolved in 5 mL of 4:1 DCM: methanol (v/v) in a round-bottom flask. The flask was connected to a rotary evaporator (Rotavapor RII, Buchi, Switzerland) at 60℃ for 1 h to evaporate DCM until completely dried. Next, the dried lipid film was hydrated in 1 mL of 0.1 mg/ml G2-RITC-NH_2 solution in ddH_2O, followed by vortexing for 15 min to form multilamellar liposomes. Multilamellar liposomes were sonicated in a bath sonicator for 30 min and then extruded 20 times through a polycarbonate membrane of 100 nm pore size using a Lipofast Pneumatic extruder (Avestin Inc., Ottawa, Canada). The resulting unilamellar liposome suspension was centrifuged at 20,000 rpm for 1 h to remove residual dendrimers. The pellet was resuspended in 1 mL of 5 % sucrose and lyophilized over 2 days.

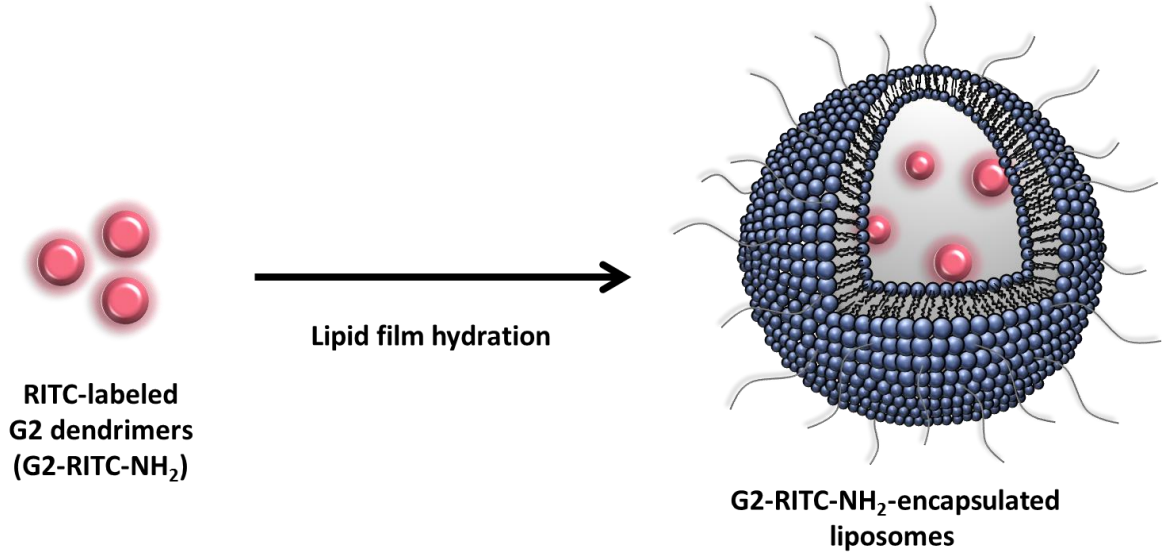

Figure 2. G2-RITC-NH_2 was encapsulated into liposomes consisting of DMPC and cholesterol. DSPE-PEG-2000 was added to enhance the stearic stability.

2.3 Characterization of dendrimer-encapsulated liposomes

Particle size (diameter, nm) and surface charge (zeta potential, mV) of the liposomes (n = 3) were obtained from quasi-elastic laser light scattering using a Nicomp 380 Zeta Potential/Particle Sizer (Particle Sizing Systems, Santa Barbara, CA) in ddH_2O. The measurements were performed using lyophilized samples that were suspended in ddH_2O at concentration of 1 mg/mL. Loading was determined by dissolving 5 mg of lyophilized liposomes in 500 µL of 0.1% Triton X-100, followed by filtration through a 0.2 µm syringe filter and measuring the fluorescence of the filtrate. The amount of dendrimers released was determined from a standard curve of dendrimer fluorescence versus concentration in 0.1% Triton X-100. Loading was calculated from the ratio of the actual measured loading to the theoretical loading (amount of dendrimers added divided by the mass of lipid and sucrose used).

2.4 Morphology of the liposomes: TEM observation

Morphology of liposomes was examined using transmission electron microscopy (TEM). Liposomes were dissolved in ddH_2O at a concentration of 1 mg/mL. 5 µL of the solution was then placed on a 300-mesh copper grid and left to dry overnight, followed by negative staining with 2% phosphotungstic acid (PTA). TEM images were acquired using a JEOL-JEM 1220 (JEOL USA) at an accelerating voltage of 80kV.

2.5 Release kinetics of G2-RITC-NH_2 from liposomes

In order to investigate the permeability of liposomes, a dendrimer release assay was conducted in PBS. A total of 10 mg of each liposome were placed in microcentrifuge tubes and dispersed in 1 mL of PBS in triplicates, and the solutions were placed in a shaking water bath (37℃, 100 rpm). At designated time points (30 min, 1h, 2, 4, 6, 8, 12, and 24 h; every 2 days thereafter), solutions were centrifuged at 14,000 rpm for 15 min, and the supernatants were collected. The liposomes were then redispersed in fresh PBS and placed back in the water bath. The fluorescence of the supernatants was measured, and the cumulative amount of dendrimers released over time was determined from a standard curve of dendrimer fluorescence versus concentration in PBS.

2.6 Cell culture

The MCF-7 cell line was obtained from ATCC (Manassas, VA) and grown continuously as a monolayer in GIBCO Dulbecco's modified Eagle's medium (DMEM, Invitrogen Corporation, Carlsbad, CA) in a humidified incubator at 37℃ and 5% CO_2. DMEM was

supplemented with penicillin (100 units/ mL), streptomycin (100 mg/ mL), and 10% heat-incubated fetal bovine serum (FBS) (Invitrogen Corporation, Carlsbad, CA) before use.

2.7 Optimization of G2 concentration for cellular uptake experiments

MCF-7 cell were seeded in 24-well plate at a density of 1×10^5 cells/well and incubated in DMEM for 24 h. G2-RITC-NH_2 was dissolved in basal DMEM at increasing concentrations: 100, 250, 500, 750, and 1000 nM. Cells were treated with the dendrimers for 3 and 6 h. Following the treatment, cells were washed with DPBS three times, followed by fixation in 200 µL of 4% paraformaldehyde for 10 min at RT. After washing the excess paraformaldehyde, 200 µL of DPBS were added and cellular uptake was visualized using an Olympus IX70 inverted microscope (IX 70-S1F2, Olympus America, Inc., Center Valley, PA).

2.8 Cellular uptake of G2-RITC-NH_2: Fluorescence Microscopy observations

MCF-7 cell were seeded in 24-well plate at a density of 1×10^5 cells/well and incubated in DMEM for 24 h. Each liposome and unencapsulated G2-RITC-NH_2 were dissolved in basal DMEM at 500 nM based on G2-RITC-NH_2. Cells were treated with the solutions for 4 and 24 h. Following the treatment, cells were washed with DPBS three times, followed by fixation in 200 µL of 4% paraformaldehyde for 10 min at RT. After washing the excess paraformaldehyde, 200 µL of DPBS were added and cellular uptake was visualized using an Olympus IX70 inverted microscope (IX 70-S1F2, Olympus America, Inc., Center Valley, PA).

2.9 Effect of low-temperature on G2-RITC-NH_2 internalization

MCF-7 cell were seeded in 24-well plate at a density of 1×10^5 cells/well and incubated in DMEM for 24 h. Each liposome and unencapsulated G2-RITC-NH_2 were dissolved in basal DMEM as described above and cells were preincubated at 4˚C for 15 min before adding the solutions. After cells were treated with the solutions at 4˚C for 4 h, cells were washed with DPBS three times, followed by fixation in 200 µL of 4% paraformaldehyde for 10 min at RT. After washing the excess paraformaldehyde, 200 µL of DPBS were added and cellular uptake was visualized using an Olympus IX70 inverted microscope (IX 70-S1F2, Olympus America, Inc., Center Valley, PA).

2.10 Cellular uptake of G2-RITC-NH_2: Flow cytometry measurements

MCF-7 cells were seeded in 12-well plates at a density of 5×10^5 cells/well and incubated in DMEM for 24 h. Cells (n = 3) were then treated with unencapsulated dendrimers and dendrimer-encapsulated liposomes with 25%, 50%, and 75% cholesterol either at 37˚C for 4 and 24 h or at 4˚C for 4 h. For low temperature experiment, cells were preincubated at 4˚C for 15 min before treated with unencapsulated dendrimers and liposomes. After each incubation period, cells were washed twice with DPBS and once with PBS, and then suspended with trypsin/EDTA. Cell suspensions were centrifuged at 3500 rpm for 5 min, resuspended in 500 µL of 1% paraformaldehyde, and transferred to flow cytometry sample tubes. Fluorescence signal intensities from the samples were measured using a Fortessa LSR (BD, Franklin Lakes, NJ), and data analysis was performed using Summit v4.3 software (Dako Colorado, Fort Collins, CO). Mean fluorescence intensity was compared using 1-way ANOVA followed by Tukey's hoc test at $p < 0.05$.

2.11 Cellular interactions of liposomes following MβCD treatment

MCF-7 cells (n = 3) were seeded in 12-well plates at a density of 5×10^5 cells/well and incubated in DMEM for 24 h and then treated with MβCD (5 mM) in basal DMEM for 1 h. After media were removed, cells were washed once with DPBS, followed by adding unencapsulated dendrimers and dendrimer-encapsulated liposomes with 25%, 50%, and 75% cholesterol at 500 nM based on G2-RITC-NH_2. The treatment was carried out for 4 and 24 h. After each incubation period, fluorescence intensities were measured by flow cytometry as described above. Mean fluorescence intensity was compared using 1-way ANOVA followed by Tukey's hoc test at $p < 0.05$.

2.12 Cytotoxicity of dendrimer-encapsulated liposomes

MCF-7 cells were seeded in 96-well plates at a density of 2×10^4 cells/well and grown in DMEM for 24 h. Cells (n = 4) were then treated with G2-RITC-NH_2 or G2-RITC-NH_2-encapsulated liposomes at concentrations of 0.1, 0.5, 1, and 10 μM based on dendrimer conjugates for 1, 4, 24, and 48 h. After each incubation time, media were removed and incubated for an additional 2 h in a normal culture condition. Cell viability was assessed using a CellTiter 96 AQueous One Solution (MTS) Assay (Promega, Madison, WI) according to the manufacturer's protocol. The UV absorbance was measured at 490 nm using a Labsystems Multiskan Plus microplate reader (Labsystems, Finland). Mean cell viabilities were determined relative to a negative control (untreated cells). Mean cell viabilities was compared using 1-way ANOVA followed by Tukey's hoc test at $p < 0.05$.

3. Results and discussion

3.1 Characterization of dendrimer-encapsulated liposomes

The particle size and zeta potential of the different liposomal formulations were measured by quasi-elastic laser light scattering in triplicates. All liposome sizes were around 170 nm in diameter. The change in zeta potential values between the liposomes (-10 mV) and G2-RITC-NH_2 (25 mV) indicated that dendrimers were successfully encapsulated into the liposomes (Table 1). Loading of G2-RITC-NH_2 was determined using a standard curve (y=138.79x + 37.416; R^2 = 0.9974) which was constructed from dendrimer fluorescence versus concentration in 0.1% Triton X-100 (Figure 3).

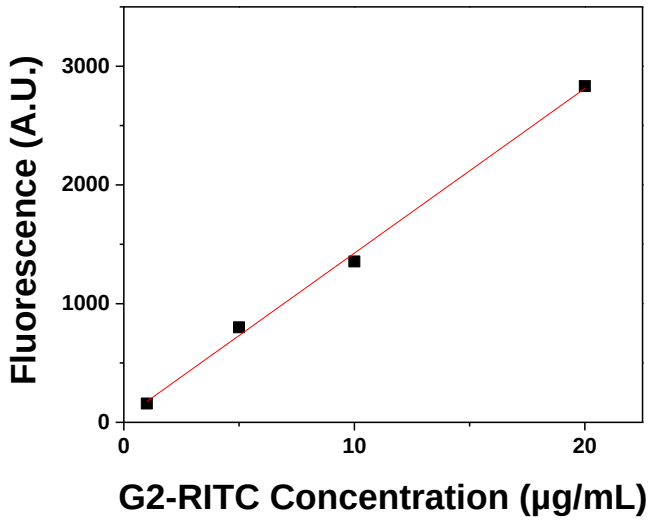

Figure 3. Standard curve generated from dendrimer fluorescence versus concentration in 0.1% Triton X-100. The standard yielded R^2 = 0.9974 and an equation y=138.79x + 37.416 (n = 1).

Table 1. Characterization of G2-RITC-NH_2-encapsulated liposomes

Formulation	25% cholesterol	50% cholesterol	75% cholesterol
Size (nm)	173.1 ± 29.1	178.2 ± 8.6	163.6 ± 12.7
Zeta potential (mV)	- 9.2 ± 12.8	- 10.1 ± 3.9	- 8.6 ± 7.6
Loading (μg/mg)	1.8 ± 0.3	2.3 ± 0.1	2.7 ± 0.3
Loading efficiency (%)	57.7 ± 10.1	72.2 ± 3.9	84.3 ± 9.1

Morphologies of the liposomes were also observed using TEM. All three liposomes were approximately in the range of 150 to 200 nm as shown in Figure 4.

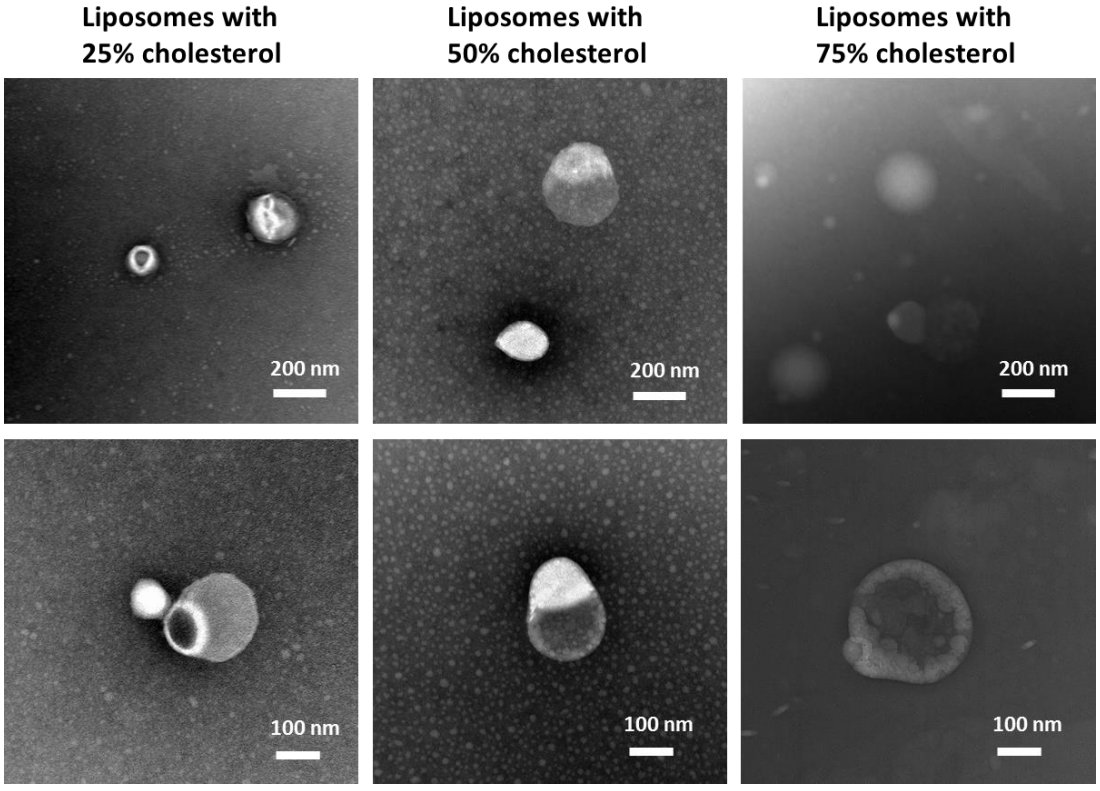

Figure 4. Transmission electron microscopy (TEM) images of dendrimer-encapsulated Liposomes (Contributed by Ryan M. Pearson)

3.2 Release kinetics of dendrimer-encapsulated liposomes

Liposome stability is essential to the efficacy of the drug delivery system since drug retention determines the release of encapsulated drugs. We first investigated the effect of cholesterol on membrane permeability of the liposomes. Membrane permeability was studied by monitoring the release of dendrimers from the three liposomal formulations: liposomes with 25%, 50%, and 75% cholesterol, in PBS. The fluorescence of the supernatants was measured, and the cumulative amount of dendrimers released over time was determined using the standard curve ($y=122.81x + 32.4$; $R^2 = 0.9994$) which was constructed from dendrimer fluorescence versus concentration in PBS (Figure 5).

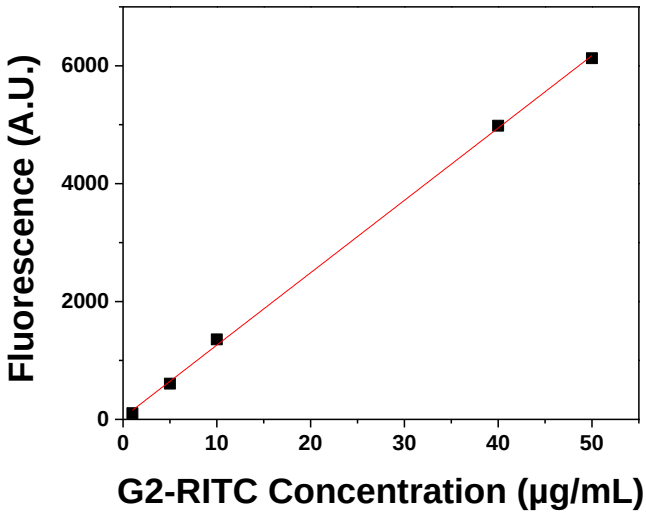

Figure 5. Standard curve generated from dendrimer fluorescence versus concentration in PBS. The standard yielded $R^2 = 0.9994$ and an equation $y=122.81x + 32.4$ (n = 1).

The release profiles of G2-RITC-NH_2 in PBS were biphasic; relatively fast release within the first few hours, and sustained profiles afterward as depicted in Figure 6a. Liposomes with 75% cholesterol showed significantly slower and sustained release kinetics; it took 36 days to release 100% of initially encapsulated dendrimers, while liposomes with 25% and 50%

cholesterol released nearly 100% dendrimers within 5 days and 14 days, respectively. Within the first hour, each liposome released almost 60% of G2-RITC-NH_2 which was probably caused by the surface desorption of dendrimers present near the liposome surface. We have previously investigated the release kinetics of RITC-labeled polyethylenimine (PEI-RITC) from liposomes consisting of DSPC, DOPG, and cholesterol (1:1:1, mole ratio). In that study, only 6% of initially encapsulated PEI-RITC into the liposome was released from liposomes within the first few hours [54]. The reason why we observed 60% leakage of G2 within the first hour could be attributed to the lipid components of liposomes. DMPC has a phase transition temperature (T_m) of 23℃ which is lower than the temperature of the release test (37℃). On the other hand, the release kinetics of PEI was obtained from liposomes which consist of DSPC, DOPG, and cholesterol. Liposomes formulated with DSPC and cholesterol have been shown to have better drug retention than liposomes formulated with DMPC due to its higher T_m (55℃) [57]. Indeed, we observed that the liposomes consisting of DSPC, DOPG, and cholesterol (1:1:1, mole ratio) released G2-RITC-NH_2 slower than liposomes consisting of DMPC and cholesterol as shown in Figure 4b. For the liposomes containing DSPC, only 30% of encapsulated G2-RITC-NH_2 was released in first 1 h, indicating that T_m of lipids is an important factor affecting the release kinetics of cargos. A possible explanation for the different release kinetics between PEI and G2-RITC-NH_2 from the same components of liposomes shown in Figure 4b is the difference in molecular weight of encapsulated materials. Molecular weight of PEI used in that study was 10,000, which is three times larger than that of G2 PAMAM dendrimers (M_w 3,256 g/mol). These differences (T_m of lipids and cargo size) might cause the different release kinetics between G2 PAMAM dendrimers and PEI.

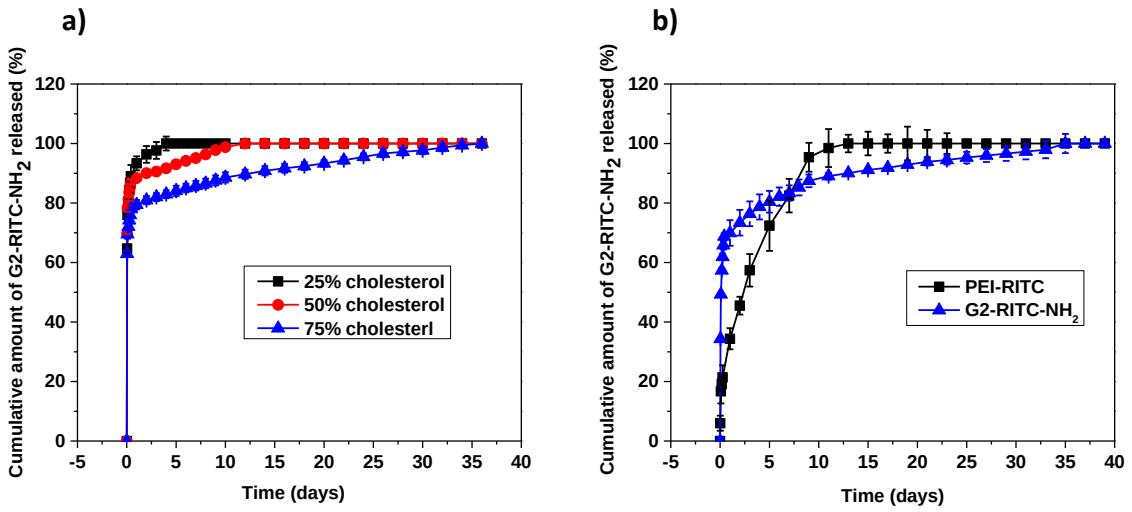

Figure 6. Release kinetics in PBS of a) G2-RITC-NH_2-encapsulated liposomes consisting of DMPC and cholesterol, and b) PEI-RITC- and G2-RITC-NH_2-encapsulated liposomes consisting of DSPC, DOPG, and cholesterol (n = 3).

3.3 Cellular uptake of dendrimer-encapsulated liposomes

First, in order to identify a dendrimer concentration for cellular uptake studies, MCF-7 cells were treated with different concentrations (100 – 1000 nM) of G2-RITC-NH_2 for 3 and 6 h. At G2-RITC-NH_2 concentrations < 250 nM, fluorescence signals were too faint to observe cellular interaction of G2-RITC-NH_2 as can be seen in Figure 7. Therefore, throughout the cellular uptake studies, we chose to treat the cells with an intermediate concentration of G2-RITC-NH_2 (500 nM), to ensure that the observations are not the result of cytotoxic interactions between the materials and the cells.

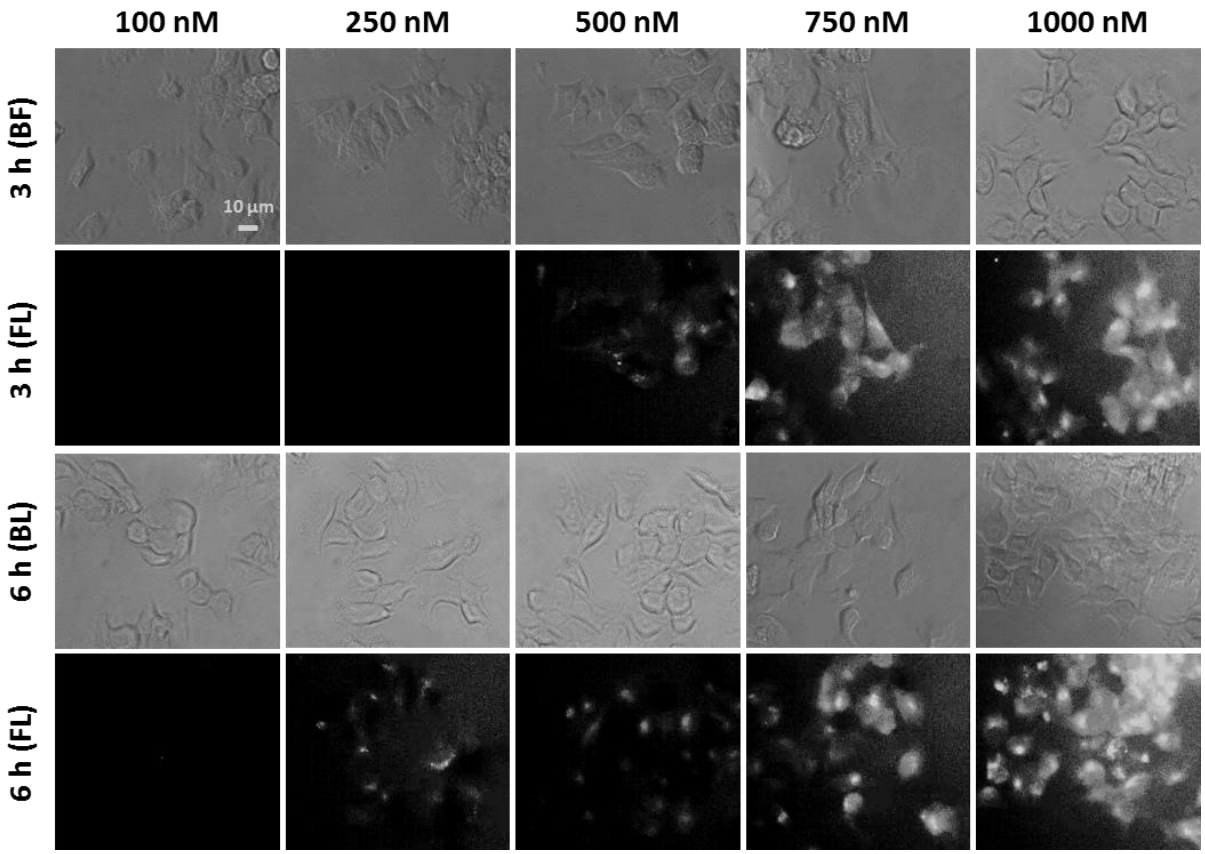

Figure 7. Cellular uptake images of different concentrations (100-100 nM) of G2-RITC-NH_2 after 3 and 6 h (BF: bright field images, FL: fluorescent images).

Next, cellular interactions of free G2-RITC-NH_2 and equivalent concentrations of the three liposomal formulations were investigated using fluorescence micrscopy. MCF-7 cells were treated with the materials for 4 and 24 h. As demonstrated in Figure 8, the fastest cellular uptake was observed from unencapsulated G2-RITC-NH_2 due to the nonspecific interaction between the cationic surface of G2-RITC-NH_2 and negatively charged cell membrane. Interestingly, liposomes with 50% and 75% cholesterol showed second fastest cellular uptake after unencapsulated G2-RITC-NH_2. This observation was not consistent with the release kinetics study in PBS; the release kinetics of G2-RITC-NH_2 was faster in the order of liposomes with 25% cholesterol, 50% cholesterol, and 75% cholesterol. Although it was expected that the liposomes with 25% cholesterol would show the faster cellular uptake, it was found that the

liposomes with 75% cholesterol exhibited faster cellular uptake, which could be explained by the cholesterol content in liposomes. We have observed that the cellular uptake of unencapsulated G2- RITC-NH_2 is always faster as shown in Figure 8, 10a, and 11a; however, in the presence of both released G2-RITC-NH_2 from liposomes and liposomes with high cholesterol content, cellular uptake of the liposomes is likely to occur faster than that of free G2-RITC-NH_2. This suggests that cholesterol-dependent endocytosis, by which liposomes internalize into the cell, is taking place faster than endocytosis of free G2-RITC-NH_2 and the kinetics of cellular uptake is highly dependent on cholesterol content in liposomes.

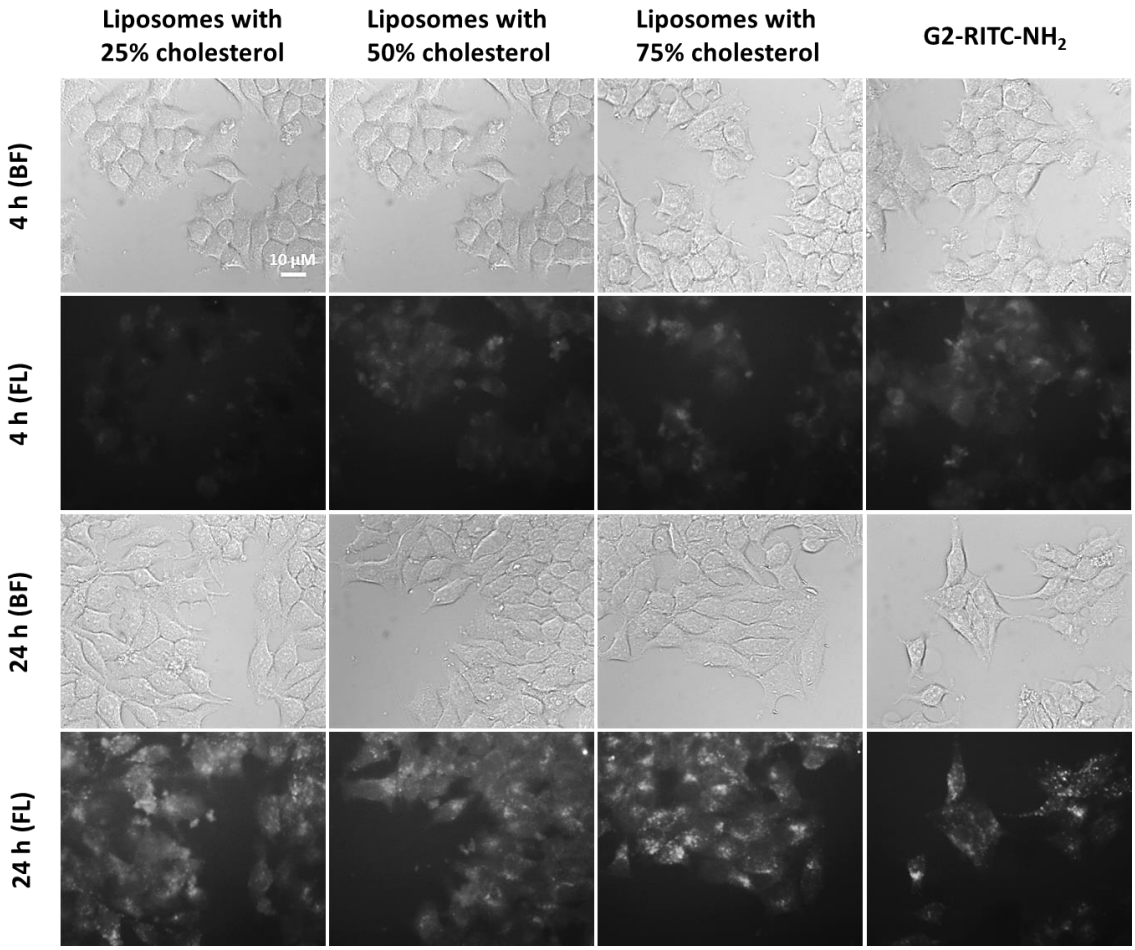

Figure 8. Cellular uptake images of MCF-7 cells following treatment with G2-RITC-NH_2 and the three liposomal formulations (liposomes with 25% cholesterol, liposomes with 50% cholesterol,

and liposomes with 75% cholesterol) at a concentration of 500 nM based on G2-RITC-NH_2 for 4 and 24 h (BF: bright field images, FL: fluorescent images).

To confirm whether the cellular uptake of unencapsulated G2-RITC-NH_2 and the three liposomal formulations is mediated by energy-dependent endocytosis, the MCF-7 cells were pre-incubated at 4℃ for 15 minutes and treated with unencapsulated G2-RITC-NH_2 and three liposomal formulations (500 nM based on G2-RITC-NH_2 concentration) for 4 h at 4℃. After incubation, no cellular interactions were observed for cells treated with G2-RITC-NH_2 as well as all three liposomal formulations at low temperature as shown in Figure 9. The flow cytometry analysis further confirmed that lowering the temperature does affect cellular uptake of both G2-RITC-NH_2 and the three liposomal formulations (Figure 10). Endocytosis of G2-RITC-NH_2 was reduced at 4℃ by 78.1% and that of liposomes with 25%, 50%, and 75% cholesterol were also suppressed by 68.4%, 76.8 %, and 75.3%, respectively. This suggests that G2-RITC-NH_2 internalization relies on energy-dependent endocytosis as well as three liposomal formulations. Generally, it is known that cationic PAMAM dendrimers bind to cells through nonspecific interactions due to their surface amine groups. The reason why cellular binding at 4˚C was hardly observed in our study could be explained by the smaller number of amine groups on G2 PAMAM dendrimers. Compared with larger generation of cationic PAMAM dendrimers such as G7, G2 PAMAM dendrimers have much less amine groups on the surface (G7: 512, G2: 16). This difference might contribute to the reason why nonspecific cellular interactions of G2-RITC-NH_2 at 4℃ were hardly observed.

Indeed, the endocytosis mechanism by which PAMAM dendrimers are internalized into cells is still debatable. For example, it has been reported by Kitchens *et al* [58] that both cationic G2

and anionic G1.5 PAMAM dendrimers are likely to internalize by clathrin-mediated endocytosis in Caco-2 cells. The mechanism was confirmed by TEM analysis showing co-localization of PAMAM dendrimers with clathrin endocytosis markers [58]. Another study has shown that anionic G4 PAMAM dendrimers are internalized by caveolae-mediated endocytosis in A549 lung epithelial cells, whereas neutral and cationic PAMAM dendrimers are internalized through a nonclathrin, noncaveolae-mediated mechanism such as electrostatic interactions or other nonspecific fluid-phase endocytosis [59]. Furthermore, Hong *et al.* has reported that although internalization of cationic G7 PAMAM dendrimers is reduced by ~60% at the lower temperature, dendrimers internalize into the cells not only at 37℃, but also at 4℃ [24]. Our results indicate that the internalization mechanism of dendrimers may not be confined to only nonspecific interactions. Therefore, it can be concluded that PAMAM dendrimer internalization and endocytosis mechanisms depend on numerous factors such as dendrimer generation, surface charge, and target cell types.

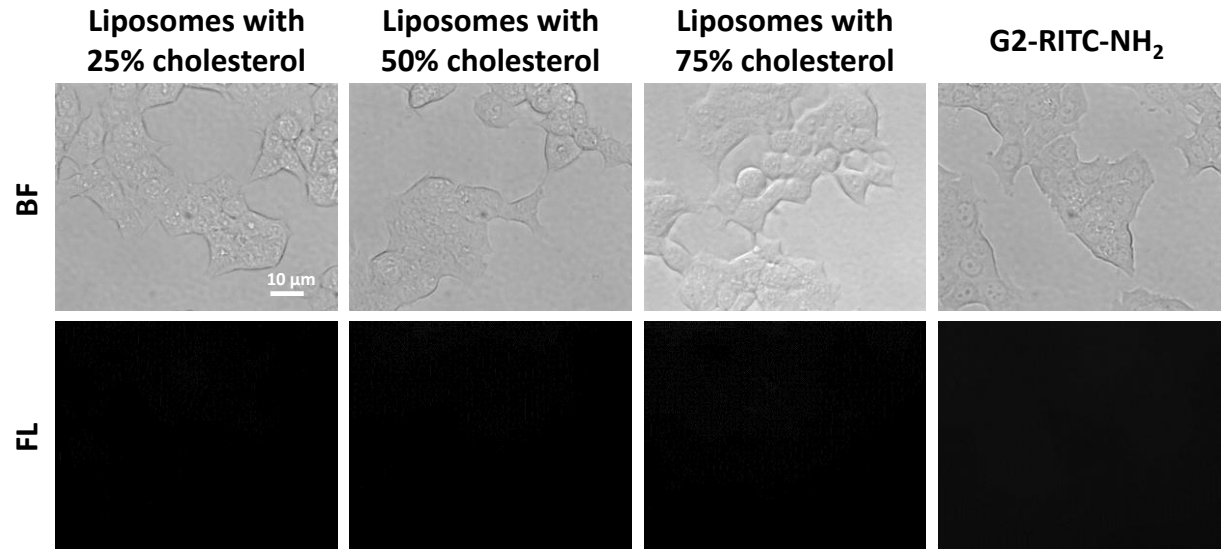

Figure 9. Cellular uptake images of G2-RITC-NH_2 and the three liposomal formulations after 4 h incubation at 4℃ (BF: bright field images, FL: fluorescent images).

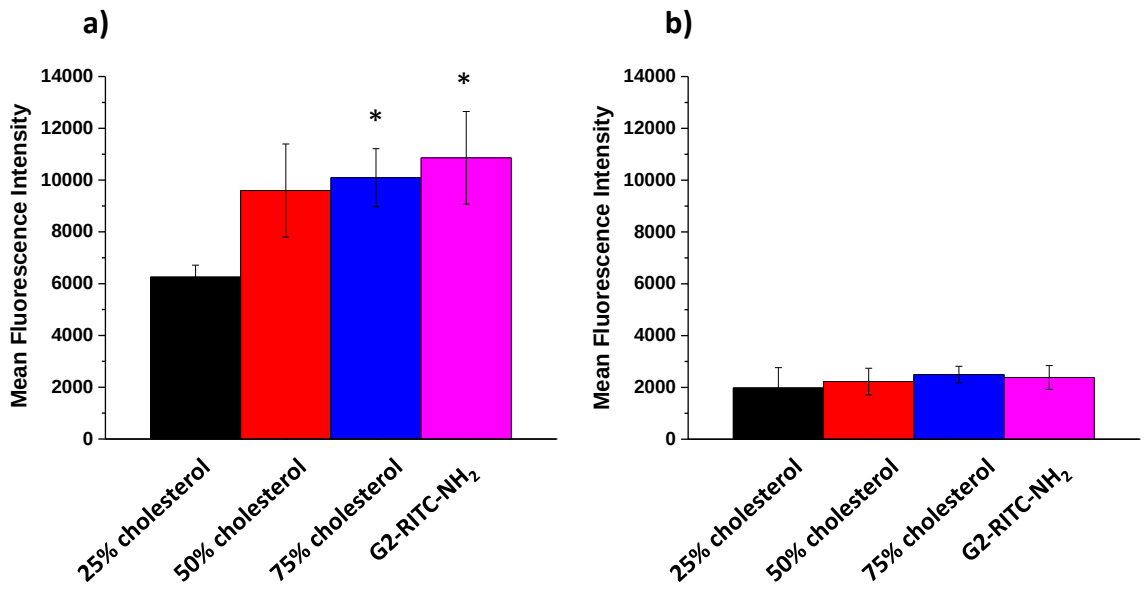

Figure 10. Cellular uptake of G2-RITC-NH_2 and the three liposomal formulations after 4 h incubation at a) 37℃ and b) 4℃ (n = 3). *Statistical significance ($p < 0.05$) between liposomes with 25% cholesterol on a 1-way ANOVA followed by Tukey's hoc test.

It has been shown that cholesterol in plasma membranes plays important roles in endocytosis of molecules [49, 60-62]. Next, in order to further clarify endocytosis mechanisms of both G2-RITC-NH_2 and liposomes, cholesterol of plasma membranes was depleted by treatment with MβCD. MβCD is a cyclic oligosaccharide and known to remove the cholesterol from the plasma membranes by lodging the hydrophobic cholesterol molecules inside cyclodextrin rings, resulting in inhibition of cholesterol-dependent endocytosis of molecules [46]. MCF-7 cells were pretreated with 5 mM MβCD for 1 h and then cellular uptake of unencapsulated G2-RITC-NH_2 and three liposomal formulations were quantified by flow cytometry as shown in Figure 11. Endocytosis after MβCD treatment was suppressed in both G2-RITC-NH_2 and all three liposomal formulations, indicating that both endocytosis mechanisms are cholesterol-dependent. For G2-RITC-NH_2, 49.6% of endocytosis was suppressed by MβCD after 24 h. Endocytosis of liposomes with 25%, 50%, and 75% cholesterol

was inhibited by 82.8%, 78.0%, and 67.7%, respectively. Compared to G2-RITC-NH_2 endocytosis inhibition, endocytosis of the three liposomal formulations was dramatically inhibited, implying the possibility of different endocytosis mechanisms between G2-RITC-NH_2 and liposomes. Generally, MβCD is used to inhibit clathrin-mediated endocytosis by depleting the cholesterol in plasma membranes. However, caveolae-mediated endocytosis is widely known to often occur at lipid rafts where cholesterol and sphingolipisds are tightly packed [63, 64]. Hence, it is still unclear which endocytosis pathway G2-RITC-NH_2 and liposomes rely on. In order to deepen the understanding of internalization mechanisms, use of different types of reagents such as filipin or rottlerin, might be needed in future studies. However, we observed differences in the degree of inhibition between G2-RITC-NH_2 and the three liposomal formulations, indicating that G2-RITC-NH_2 is internalized through a different endocytosis mechanism from liposomes.

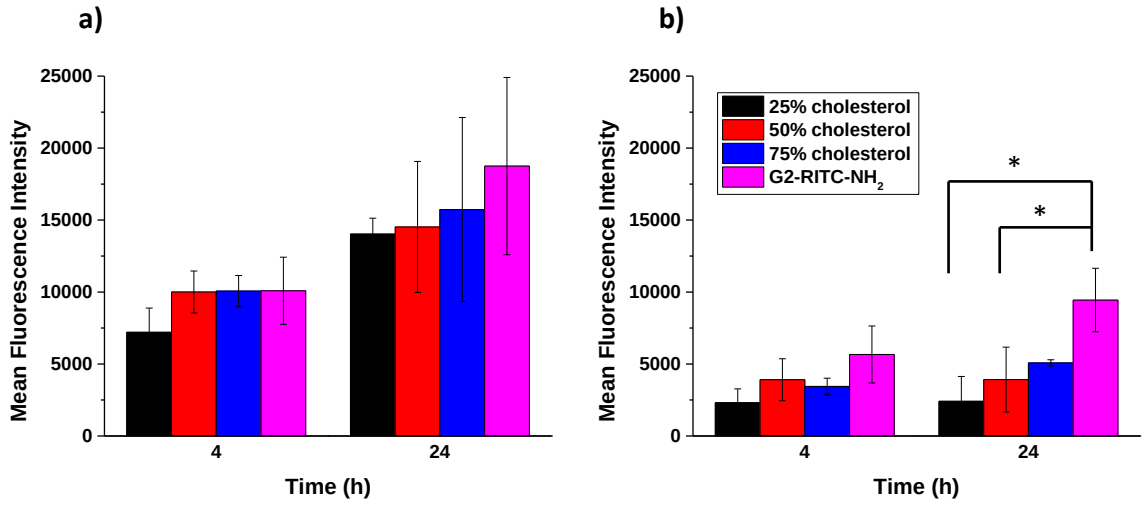

Figure 11. Cellular uptake of G2-RITC-NH_2 and the three liposomal formulations in the a) absence and b) presence of MβCD (n = 3). *Statistical significance ($p < 0.05$) on the basis of a 1-way ANOVA followed by Tukey's hoc test.

3.4 Cytotoxicity of dendrimers and dendrimer-encapsulated liposomes

We investigated the *in vitro* cytotoxicity of free G2-RITC-NH_2 and G2-RITC-NH_2-encapsulated liposomes with 25%, 50%, or 75% cholesterol on MCF-7 cells at different dendrimer concentrations. As shown in Figure 12, none of the liposomal formulations showed any cytotoxicity after 48 h over the concentrations tested. On the other hand, cytotoxicity of amine-terminated PAMAM dendrimers is generally known to arise due to their cationic surface charge, creating hole formation in lipid bilayers and resulting in cell death [23]. However, no significant inhibition in cell proliferation was observed in cells treated with free G2-RITC-NH_2 even after 48 h of incubation as shown in Figure 12. This can be explained by the fact that the cytotoxicity of PAMAM dendrimers is highly dependent on their size [23, 24]. As mentioned previously, G2 PAMAM dendrimers have only 16 amine groups on the surface, while G7 PAMAM dendrimers have 512 amine groups. It has been reported that amine terminated 400 nM of G7 PAMAM dendrimers starts showing a degree of cytotoxicity (~20% toxicity) [24]; on the other hand, G2-RITC-NH_2 is better tolerated by the cells even at concentrations as high as 10 μM.

We further tested the cytotoxicity of higher concentrations of free G2-RITC-NH_2 as shown in Figure 13. Both 100 and 500 μM of G2-RITC-NH_2 start to exhibit cytotoxicity after 4 h, as indicated by reduction in cell viability relative to untreated controls (<80% for 100 μM and <60% for 500 μM). The result suggests that a liposomal formulation of G2 PAMAM dendrimers is well tolerated up to micromolar concentrations and has the potential to be used as a drug delivery carrier.

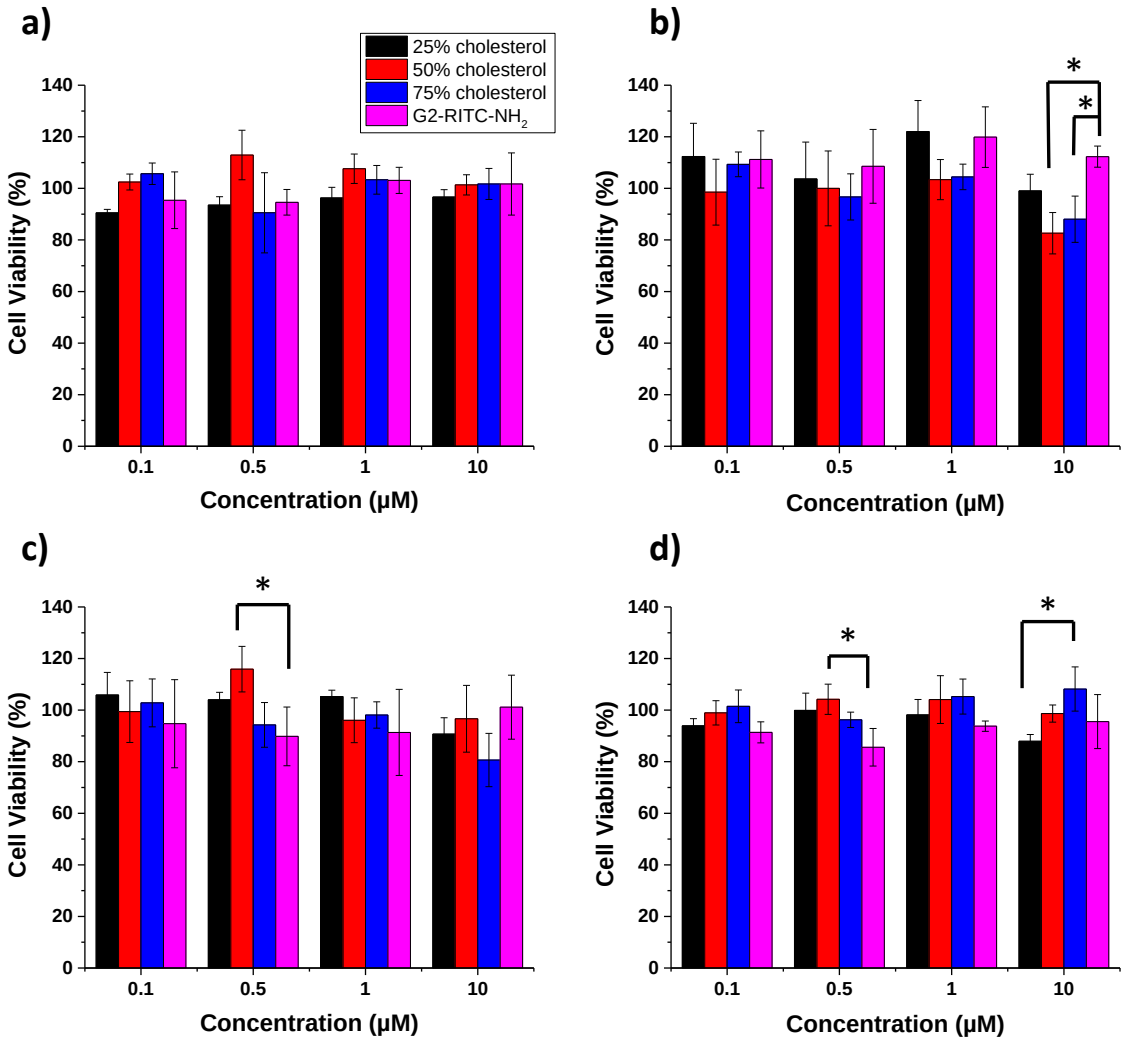

Figure 12. Cytotoxicity of G2-RITC-NH_2 and G2-RITC-NH_2-encapsulated liposomes after incubation with MCF-7 cells for a) 1 h, b) 4 h, c) 24 h, and d) 48 h at a concentration equivalent to 0.1, 0.5, 1, and 10 μM G2-RITC-NH_2 (n = 3). *Statistical significance ($p < 0.05$) on the basis of a 1-way ANOVA followed by Tukey's hoc test.

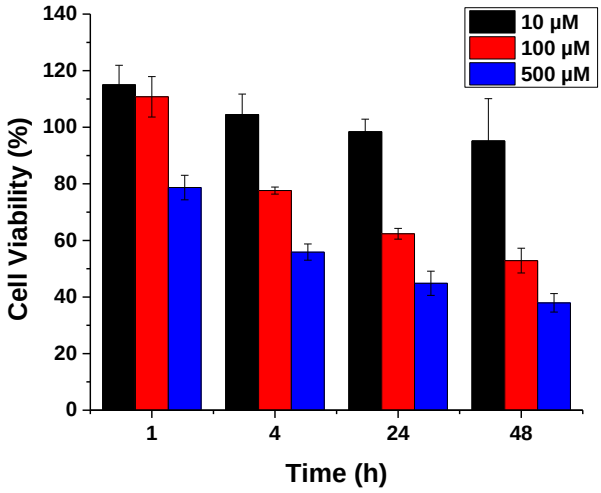

Figure 13. Cytotoxicity of G2-RITC-NH_2 after incubation with MCF-7 cells at concentrations of 10, 100, and 500 μM up to 48 h (n = 3).

4. Conclusion

In this study, we tested the feasibility of encapsulating G2 PAMAM dendrimers into liposomes, and investigated the effect of lipid composition on their *in vitro* properties. G2-RITC-NH_2 was encapsulated into three different liposomal formulations (liposomes with 25%, 50%, and 75% cholesterol) and their release kinetics, cellular interactions, and cytotoxicity were investigated. Release tests revealed that the amount of cholesterol in liposomal membranes strongly affect the membrane permeability, as we observed faster release of G2-RITC-NH_2 from liposomes with 25% cholesterol while G2-RITC-NH_2 was released much slower from liposomes with 75% cholesterol (Figure 6a). For the cellular uptake study, microscope observation and flow cytometry analysis showed that G2-RITC-NH_2-encapsulated lipsosomes with 75% cholesterol internalized faster than the other liposomal formulations. Furthermore, inhibition of cellular uptake of the liposomes in cells pretreated with MβCD suggested that these liposomes are taken up by cholesterol-dependent endocytosis, whereas unencapsulated G2-RITC-NH_2 internalized utilizing both energy dependent endocytosis and nonspecific interactions.
As shown in Figures 8, 10a, and 11a, faster cellular interaction is always observed in the cells treated with unencapsulated G2-RITC-NH_2 due to their different cellular interaction mechanisms from liposomes. We observed that membranes of liposome with 25% cholesterol are more permeable compared with that of cholesterol rich liposomes (Figure 6a), indicating that faster cellular uptake of released G2-RITC-NH_2 from liposomes should be exhibited in the cells treated with 25% cholesterol, followed by the cells incubated with unencapsulated G2-RITC-NH_2. However, our cellular uptake images and flow cytometry measurements suggested that internalization occurred in the order of unencapsulated G2-RITC-NH_2, liposomes with 75%, 50%, and 25% cholesterol. These results indicate that cholesterol in liposomes contributes to

their faster cellular uptake when unencapuslated G2-RITC-NH_2 and cholesterol rich liposomes are coexisted.

Taken together, the results of this study reveal that the lipid composition impacts the stability and cellular interactions of the dendrimer-encapsulated liposomes. This proof-of-concept study clearly shows the potential of this delivery platform that combines the advantages of liposomes and dendrimers.

References

1. *Cancer Facts & Figures*. 2013, American Cancer Society, Atlanta.
2. Peer, D., et al., *Nanocarriers as an emerging platform for cancer therapy.* Nature Nanotechnology, 2007. **2**(12): p. 751-760.
3. Petros, R.A. and J.M. DeSimone, *Strategies in the design of nanoparticles for therapeutic applications.* Nature Reviews Drug Discovery, 2010. **9**(8): p. 615-627.
4. Zhang, L., et al., *Nanoparticles in Medicine: Therapeutic Applications and Developments.* Clin Pharmacol Ther, 2007. **83**(5): p. 761-769.
5. Ferrari, M., *Cancer nanotechnology: opportunities and challenges.* Nat Rev Cancer, 2005. **5**(3): p. 161-171.
6. Davis, M.E., Z. Chen, and D.M. Shin, *Nanoparticle therapeutics: an emerging treatment modality for cancer.* Nature Reviews Drug Discovery, 2008. **7**(9): p. 771-782.
7. Shi, J., et al., *Nanotechnology in Drug Delivery and Tissue Engineering: From Discovery to Applications.* Nano Letters, 2010. **10**(9): p. 3223-3230.
8. Farokhzad, O.C. and R. Langer, *Nanomedicine: Developing smarter therapeutic and diagnostic modalities.* Advanced Drug Delivery Reviews, 2006. **58**(14): p. 1456-1459.
9. Folkman, J., *Angiogenesis in cancer, vascular, rheumatoid and other disease.* Nat Med, 1995. **1(1)**: p. 27-30.
10. Matsumura, Y. and H. Maeda, *A new concept for macromolecular therapeutics in cancer chemotherapy: mechanism of tumoritropic accumulation of proteins and the antitumor agent smancs.* Cancer Research, 1986. **46**(12): p. 6387-6392.
11. Maeda, H., *Tumor-Selective Delivery of Macromolecular Drugs via the EPR Effect: Background and Future Prospects.* Bioconjugate Chemistry, 2010. **21**(5): p. 797-802.
12. Hobbs, S.K., et al., *Regulation of transport pathways in tumor vessels: Role of tumor type and microenvironment.* Proceedings of the National Academy of Sciences of the United States of America, 1998. **95**(8): p. 4607-4612.
13. Couvreur, P. and C. Vauthier, *Nanotechnology: Intelligent design to treat complex disease.* Pharmaceutical Research, 2006. **23**(7): p. 1417-1450.
14. Bae, Y.H., *Drug targeting and tumor heterogeneity.* Journal of Controlled Release, 2009. **133**(1): p. 2-3.
15. Kukowska-Latallo, J.F., et al., *Nanoparticle targeting of anticancer drug improves therapeutic response in animal model of human epithelial cancer.* Cancer Research, 2005. **65**(12): p. 5317-5324.
16. Esfand, R. and D.A. Tomalia, *Poly(amidoamine) (PAMAM) dendrimers: from biomimicry to drug delivery and biomedical applications.* Drug Discovery Today, 2001. **6**(8): p. 427-436.
17. Tomalia, D.A. and J.M.J. Frechet, *Discovery of dendrimers and dendritic polymers: A brief historical perspective.* Journal of Polymer Science Part a-Polymer Chemistry, 2002. **40**(16): p. 2719-2728.
18. Maruyama-Tabata, H., et al., *Effective suicide gene therapy in vivo by EBV-based plasmid vector coupled with polyamidoamine dendrimer.* Gene Therapy, 2000. **7**(1): p. 53-60.
19. Menjoge, A.R., R.M. Kannan, and D.A. Tomalia, *Dendrimer-based drug and imaging conjugates: design considerations for nanomedical applications.* Drug Discovery Today, 2010. **15**(5-6): p. 171-185.

20. Lee, C.C., et al., *Designing dendrimers for biological applications.* Nat Biotech, 2005. **23**(12): p. 1517-1526.
21. Svenson, S. and D.A. Tomalia, *Dendrimers in biomedical applications—reflections on the field.* Advanced Drug Delivery Reviews, 2005. **57**(15): p. 2106-2129.
22. Hong, S.P., et al., *Interaction of poly(amidoamine) dendrimers with supported lipid bilayers and cells: Hole formation and the relation to transport.* Bioconjugate Chemistry, 2004. **15**(4): p. 774-782.
23. Hong, S.P., et al., *Interaction of polycationic polymers with supported lipid bilayers and cells: Nanoscale hole formation and enhanced membrane permeability.* Bioconjugate Chemistry, 2006. **17**(3): p. 728-734.
24. Hong, S., et al., *The Role of Ganglioside GM(1) in Cellular Internalization Mechanisms of Poly(amidoamine) Dendrimers.* Bioconjugate Chemistry, 2009. **20**(8): p. 1503-1513.
25. Torchilin, V.P., *Recent advances with liposomes as pharmaceutical carriers.* Nat Rev Drug Discov, 2005. **4**(2): p. 145-160.
26. Harashima, H., Y. Shinohara, and H. Kiwada, *Intracellular control of gene trafficking using liposomes as drug carriers.* European Journal of Pharmaceutical Sciences, 2001. **13**(1): p. 85-89.
27. Mitchell, N., et al., *Incorporation of paramagnetic, fluorescent and PET/SPECT contrast agents into liposomes for multimodal imaging.* Biomaterials, 2013. **34**(4): p. 1179-1192.
28. Kamaly, N., et al., *Folate Receptor Targeted Bimodal Liposomes for Tumor Magnetic Resonance Imaging.* Bioconjugate Chemistry, 2009. **20**(4): p. 648-655.
29. Gabizon, A.A., *Pegylated liposomal doxorubicin: Metamorphosis of an old drug into a new form of chemotherapy.* Cancer Investigation, 2001. **19**(4): p. 424-436.
30. Gabizon, A., H. Shmeeda, and Y. Barenholz, *Pharmacokinetics of pegylated liposomal doxorubicin - Review of animal and human studies.* Clinical Pharmacokinetics, 2003. **42**(5): p. 419-436.
31. Nie, Y., et al., *Cholesterol Derivatives Based Charged Liposomes for Doxorubicin Delivery: Preparation, In Vitro and In Vivo Characterization.* Theranostics, 2012. **2**(11): p. 1092-1103.
32. Barenholz, Y., *Doxil (R) - The first FDA-approved nano-drug: Lessons learned.* Journal of Controlled Release, 2012. **160**(2): p. 117-134.
33. Gabizon, A., et al., *Prolonged Circulation Time and Enhanced Accumulation in Malignant Exudates of Doxorubicin Encapsulated in Polyethylene-glycol Coated Liposomes.* Cancer Research, 1994. **54**(4): p. 987-992.
34. Solomon, R. and A.A. Gabizon, *Clinical pharmacology of liposomal anthracyclines: Focus on pegylated liposomal doxorubicin.* Clinical Lymphoma & Myeloma, 2008. **8**(1): p. 21-32.
35. Lipworth, A.D., C. Robert, and A.X. Zhu, *Hand-Foot Syndrome (Hand-Foot Skin Reaction, Palmar-Plantar Erythrodysesthesia): Focus on Sorafenib and Sunitinib.* Oncology, 2009. **77**(5): p. 257-271.
36. Lee, S.C., et al., *The effect of cholesterol in the liposome bilayer on the stabilization of incorporated retinol.* Journal of Liposome Research, 2005. **15**(3-4): p. 157-166.
37. de Kruyff, B., R.A. Demel, and L.L.M. dan Deenen, *The effect of cholesterol and epicholesterol incorporation on the permeability and on the phase transition of intact Acholeplasma laidlawii cell membranes and derived liposomes.* Biochimica et Biophysica Acta (BBA) - Biomembranes, 1972. **255**(1): p. 331-347.

38. Tseng, L.-P., *Liposomes Incorporated with Cholesterol for Drug Release Triggered by Magnetic Field.* Journal of Medical and Biological Engineering, 2007. **27**(1): p. 29-34.
39. De Gier, J., J.G. Mandersloot, and L.L.M. Van Deenen, *Lipid composition and permeability of liposomes.* Biochimica et Biophysica Acta (BBA) - Biomembranes, 1968. **150**(4): p. 666-675.
40. Senior, J. and G. Gregoriadis, *Stability of small unilamellar liposomes in serum and clearance from the circulation: The effect of the phospholipid and cholesterol components.* Life Sciences, 1982. **30**(24): p. 2123-2136.
41. Bloch, K., *Chapter 12 Cholesterol: evolution of structure and function*, in *New Comprehensive Biochemistry*, E.V. Dennis and E.V. Jean, Editors. 1991, Elsevier. p. 363-381.
42. Brown, M.S. and J.L. Goldstein, *Multivalent feedback regulation of HMG CoA reductase, a control mechanism coordinating isoprenoid synthesis and cell growth.* Journal of Lipid Research, 1980. **21**(5): p. 505-517.
43. Reinhart, M.P., et al., *Subcellular localization of the enzymes of cholesterol biosynthesis and metabolism in rat liver.* Journal of Biological Chemistry, 1987. **262**(20): p. 9649-9655.
44. Lange, Y., *Disposition of intracellular cholesterol in human fibroblasts.* Journal of Lipid Research, 1991. **32**(2): p. 329-39.
45. Rothberg, K.G., et al., *Cholesterol controls the clustering of the glycophospholipid-anchored membrane receptor for 5-methyltetrahydrofolate.* Journal of Cell Biology, 1990. **111**(6): p. 2931-2938.
46. Rodal, S.K., et al., *Extraction of Cholesterol with Methyl-β-Cyclodextrin Perturbs Formation of Clathrin-coated Endocytic Vesicles.* Molecular Biology of the Cell, 1999. **10**(4): p. 961-974.
47. Hailstones, D., et al., *Regulation of caveolin and caveolae by cholesterol in MDCK cells.* Journal of Lipid Research, 1998. **39**(2): p. 369-379.
48. Parton, R.G., B. Joggerst, and K. Simons, *Regulated internalization of caveolae.* Journal of Cell Biology, 1994. **127**(5): p. 1199-1215.
49. Imelli, N., et al., *Cholesterol is required for endocytosis and endosomal escape of adenovirus type 2.* Journal of Virology, 2004. **78**(6): p. 3089-3098.
50. Cossec, J.C., et al., *Clathrin-dependent APP endocytosis and A beta secretion are highly sensitive to the level of plasma membrane cholesterol.* Biochimica Et Biophysica Acta-Molecular and Cell Biology of Lipids, 2010. **1801**(8): p. 846-852.
51. Purohit, G., T. Sakthivel, and A.T. Florence, *Interaction of cationic partial dendrimers with charged and neutral liposomes.* International Journal of Pharmaceutics, 2001. **214**(1-2): p. 71-76.
52. Khopade, A.J., et al., *Effect of dendrimer on entrapment and release of bioactive from liposomes.* International Journal of Pharmaceutics, 2002. **237**(1-2): p. 251-253.
53. Gardikis, K., et al., *New Drug Delivery Nanosystem Combining Liposomal and Dendrimeric Technology (Liposomal Locked-In Dendrimers) for Cancer Therapy.* Journal of Pharmaceutical Sciences, 2010. **99**(8): p. 3561-3571.
54. Sunoqrot, S., et al., *Kinetically Controlled Cellular Interactions of Polymer-Polymer and Polymer-Liposome Nanohybrid Systems.* Bioconjugate Chemistry, 2011. **22**(3): p. 466-474.

55. Sunoqrot, S., et al., *Temporal Control over Cellular Targeting through Hybridization of Folate-targeted Dendrimers and PEG-PLA Nanoparticles.* Biomacromolecules, 2012. **13**(4): p. 1223-1230.
56. Yang, Y., et al., *Effect of Size, Surface Charge, and Hydrophobicity of Poly(amidoamine) Dendrimers on Their Skin Penetration.* Biomacromolecules, 2012. **13**(7): p. 2154-2162.
57. Anderson, M. and A. Omri, *The effect of different lipid components on the in vitro stability and release kinetics of liposome formulations.* Drug Delivery, 2004. **11**(1): p. 33-39.
58. Kitchens, K.M., et al., *Endocytosis and interaction of poly (amidoamine) dendrimers with Caco-2 cells.* Pharmaceutical Research, 2007. **24**(11): p. 2138-2145.
59. Perumal, O.P., et al., *The effect of surface functionality on cellular trafficking of dendrimers.* Biomaterials, 2008. **29**(24-25): p. 3469-3476.
60. Takahashi, M., et al., *Cholesterol controls lipid endocytosis through Rab11.* Molecular Biology of the Cell, 2007. **18**(7): p. 2667-2677.
61. Zuhorn, I.S., R. Kalicharan, and D. Hoekstra, *Lipoplex-mediated transfection of mammalian cells occurs through the cholesterol-dependent clathrin-mediated pathway of endocytosis.* Journal of Biological Chemistry, 2002. **277**(20): p. 18021-18028.
62. Sharma, D.K., et al., *Selective stimulation of caveolar endocytosis by glycosphingolipids and cholesterol.* Molecular Biology of the Cell, 2004. **15**(7): p. 3114-3122.
63. Pantos, A., et al., *Interaction of functional dendrimers with multilamellar liposomes: Design of a model system for studying drug delivery.* Langmuir, 2005. **21**(16): p. 7483-7490.
64. Brown, D.A. and E. London, *Functions of lipid rafts in biological membranes.* Annual Review of Cell and Developmental Biology, 1998. **14**(1): p. 111-136.

Vita

Name: Eri Iwasaki

Education: M.S., Bioengineering at University of Illinois at Chicago (2013)
Thesis – Preparation and In Vitro Analysis of Dendrimer-encapsulated Liposomes
B.S., Applied Chemistry, Ehime University (2009)

Professional Organizations: Alpha Eta Mu Beta (AEMB)